

ROTOR LIFE PREDICTION AND IMPROVEMENT FOR STEAM TURBINES UNDER CYCLIC OPERATION

Damaso Checcacci
GE Oil & Gas
Nuovo Pignone
Florence, Italy

Lorenzo Cosi
GE Oil & Gas
Nuovo Pignone
Florence, Italy

Sanjay Kumar Sah
GE Oil & Gas
J.F. Welch Technology Centre
Bangalore, Karnataka, India

ABSTRACT

The evolution of the energy market is leading to a general increase in demand for cyclic operation and rapid startup capability for steam turbines utilized in power utility plants.

As a consequence, turbine manufactures must optimize designs to minimize transient stress and make available to plant operators the necessary understanding of the impact of operating conditions on parts life.

In addition, if continuous duty operation is not economical for an existing plant, operators considering switching to the cyclic mode need to take into account the cost associated with reduced maintenance intervals and parts replacement.

This paper presents the methodologies applied to assess and optimize steam turbine rotor life. The discussion stems from the case analysis of a 60 MW steam turbine that was operated almost uninterrupted for 10 years in a combined cycle plant and was then expected to switch to cyclic operation with approx 250 startups/year.

The effects of different rotor geometries on transient thermal stress/strain conditions are presented along with the consequences of startup sequence modifications for rotor life vs. on-line time.

The discussion is supported by modeling details and results from transient thermomechanical FEM analyses. The possibility of a simplified approach in the form of approximate models for the analysis of such behavior on a project basis is also addressed.

1 INTRODUCTION

Steam turbines are the backbone of the power generation industry and currently generate 80% of the world's electrical energy. Power generation steam turbines have been used in fossil (coal, oil or natural gas), nuclear, geothermal, combined cycle and biomass power plants. The majority of these applications have been for continuous operation and

steady load. Since they were not started frequently, startup time was not a critical requirement and thermal stresses were managed by loading the unit slowly.

Cyclic operation was required for some combined cycle steam turbines utilized in peaking power plants. The growth of discontinuous energy sources like wind or solar are increasing the need for flexible plants capable of compensating for the oscillation associated with renewable source energy production. In some cases, the fluctuation of the energy and gas price balance can also oblige operators to shut down combined cycle turbines at night when the decrease in energy price outweighs the cost of the gas. As a consequence, plants conceived for steady operations are sometimes required to switch to the cyclic mode of operation.

In these cases, turbine manufactures must re-assess existing steam turbine capabilities, taking into account the cyclic operation duty cycle. This not only includes the retrieval of information or assumptions on experience on startup cycles, but also aspects such as material aging and a deep understanding of the status of critical parts.

Concentrated Solar Plants (CSP) have rapidly expanded in the last 5 years[1]. Steam turbines used in these plants are exposed to daily start up and continuous load variations as a function of the solar radiation.

The combination of all the factors discussed above is strongly increasing the demand for cyclic operation capability in steam turbines.

Cyclic application imposes conflicting requirements on the design and operation of new steam turbines. Optimization of the maintenance interval and parts life management become critical for the economics of the plant operation. Understanding and control of the startup transient stress is the key point to assess components life correctly. The logical way to reduce thermal stress would be to start the unit slowly as it was done in the past. This approach is no longer economically viable since by increasing the number of starts per year, the amount of

energy produced during the startups becomes a significant portion of the total. To maximize it, manufacturers are asked to reduce the total startup time and increase the slope of the load ramp.

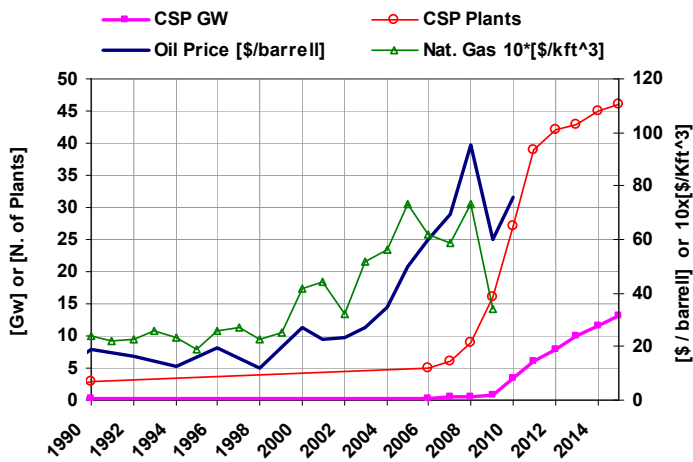


Fig.1 Left axis : CSP installations and GWs (based on installed and proposed plants). Right axis : historical prices for Oil and Natural gas Ref.[1],[2].

In the following, starting from the case study analysis of a steam turbine rotor for combined cycle application, the concurrence of factors affecting unit life are discussed in view of the overall plant profitability.

2 NOMENCLATURE

- CSP : concentrated solar plant
- DCS : distributed control system
- FEM : Finite Element Method
- HP : high pressure
- K_m : equivalence factor for mechanical loads
- K_{th} : equivalence factor for thermal loads
- LCF : low cycle fatigue
- LP : low pressure
- MP : medium pressure
- σ_{em} , σ_{eM} : minimum and maximum Von Mises equivalent stress
- t_L : final load ramp time
- t_p : pre-load time
- t_w : warm-up time

3 CASE STUDY

3.1 General Data

The unit under investigation in this section is a 60[MW]-50[Hz] condensing reaction seam turbine installed at the end of the '90s in a combined cycle plant and operated mostly continuously with inlet steam conditions of 485[°C], 77 [bara] and exhaust conditions of 36[°C] and 0.06 [bara].

Due to the upcoming expiration of the contractual agreement for the price of electrical energy between the plant owner and the local national energy agency, the plant is foreseen to be operated on the basis of daily profitability as resulting from natural gas and electricity market prices.

The goal of the study was the identification of the effects on rotor life of an increase from approximately 20 starts/year to 200-250, based on a stop almost each weeknight and a longer stop over the week-end to follow the price of electricity.

The rotor under consideration is a drum type design, full bore, 31[tons] and 6500[mm] length; its general assembly is depicted in Figure 2. There is no control stage and the steam, following the HP inner casing cavity, is sent directly from the inlet valves to the first stage nozzles through a 360° annulus. The HP section consists of three drums, while a 4th drum, just after the extraction, serves as a separation between the HP and MP/LP sections. There are a total of 54 stages.

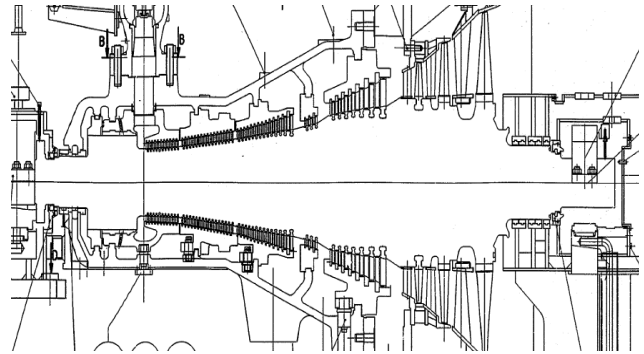


Fig.2 General arrangement of the rotor

3.2 Mission

The mission analysis was conducted on the basis of the requirements from the operating manual and DCS logs from the field. The startup sequence consists of three main phases:

- 1) a warm up phase at low speed, held for a time t_w ;
- 2) acceleration up to synchronization and operation at reduced load for an overall time t_p ;
- 3) final load ramp, to reach 100% load over a time t_L .

This baseline startup sequence is depicted in Fig.3.

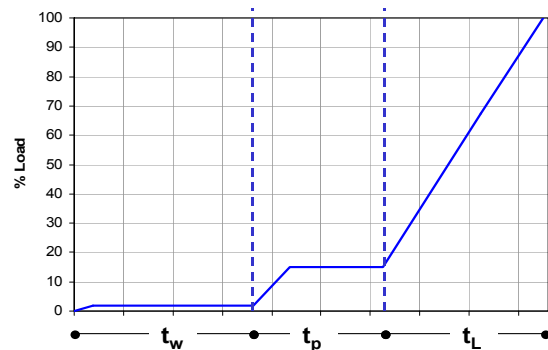


Fig.3 Reference baseline startup sequence

For a hot startup, both t_w and t_p are reduced to shaft acceleration times, while the load ramp is increased by reducing t_L accordingly. These times depend on the machine size and, in this work, the reference times for the baseline cycle will be defined as t_{w0} , t_{p0} and t_{L0} .

The field data showed that this startup sequence was respected, apart from a few deviations of the final load ramp related to steam extraction.

3.3 Critical geometric parameters

The study was primarily aimed at investigating the distribution of stresses at critical locations for the drum rotors, such as balance drum fillets and bucket dovetail grooves at the first stages. For this particular unit, these had the geometry depicted in Figure 4.

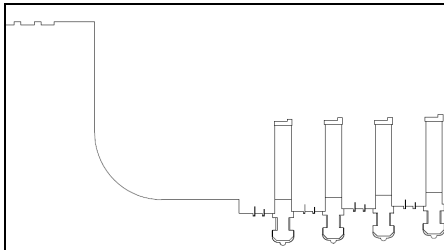


Fig.4 Detail of blade dovetails and rotor grooves for baseline.

The blades have T root dovetails and the corresponding rotor groove has an additional semicircular groove for radial locking crush pins.

4 BASELINE RESULTS

4.1 Thermal distributions

A thermal analysis was conducted starting from cold and hot conditions up to steady state. Cool-down after shutdown was also simulated, including modeling of the casing, to match the casing temperature data from the field and correctly match the starting conditions for cold, warm and hot restarts.

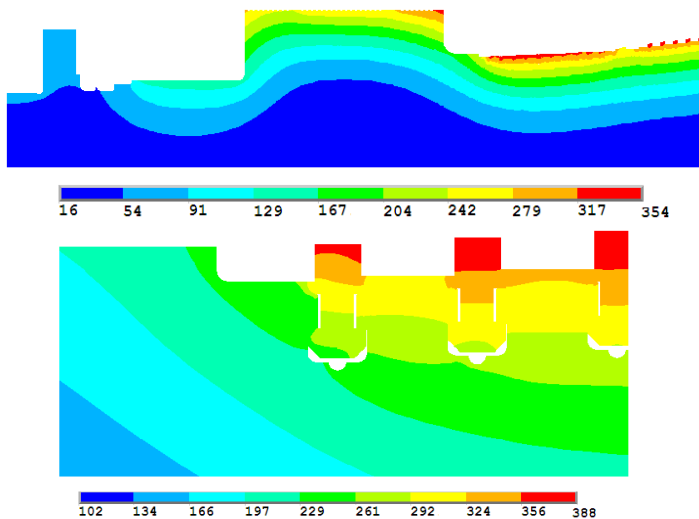


Fig.5 Temperature [°C] in balance drum area at $t = 850[s]$ and detail of first stage dovetails.

In Fig.5 the transient thermal distributions for cold start at $15[°C]$ are reported at $850[s]$ from start. The balance drum portion is represented along with a detail of the temperatures at the first stage dovetails, where a thermal bridge effect is

evident. The airfoil, exposed to hot steam flow, experiences a fast temperature increase and the blade dovetail increases its temperature faster than the surrounding shaft material. The crush pin (not represented in the figure) in turn conveys this heat to the shaft groove, generating a faster increase in the local temperature.

In Fig.6, the steady state thermal distribution is reported (approximately eight hours from start), showing that the balance drum and first stages reached approximately $480°C$ and no thermal gradient is present in the radial direction.

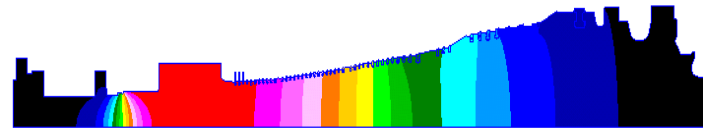


Fig.6 Temperature distribution along the rotor at steady state (15 to $480°C$).

4.2 Mechanical results

The elastic analysis of the baseline case showed that the peak stress was reached at $850[s]$ at the bottom of the groove for the crush pin. This stress pattern is typical for all dovetail grooves and is driven by two main factors: a global radial gradient effect and a local amplification factor.

Globally, the radial thermal gradient produces axial thermal expansion of the outer material layers. At the outer surface, the material is free to expand axially between successive grooves, while closer to the groove bottom depth, this axial expansion is impeded by deeper layers. As a consequence, the thermal axial expansion of the groove walls produces a compressive stress concentration at the bottom of the groove itself (Fig.7).

Local effects add to this global behavior. Indeed, the semicircular crush pin groove produces an additional geometrical notch factor for stresses in the axial direction, and, as discussed in par. 4.1, the crush pin itself acts as a thermal bridge increasing the local shaft temperature.

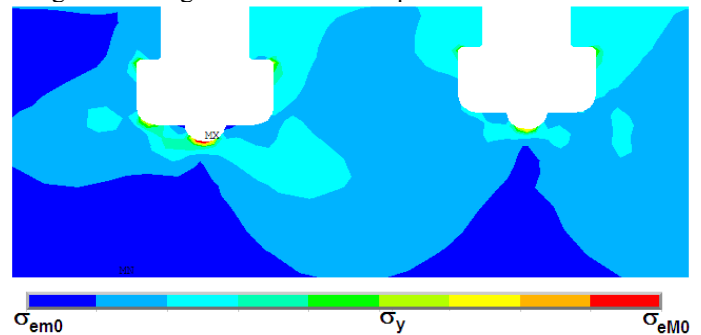


Fig.7 Elastic distribution of stresses at groove dovetail bottom

To this point, it should be noted that the peak stress is reached at the moment of maximum difference between the crush pin groove and the outer shaft temperatures (Fig.5).

The overall effects are exemplified in Fig.8, where the comparison of the relative contribution of the stress components is provided, showing how compressive axial stress is the predominant stress, and radial stress does not affect the critical groove area at all.

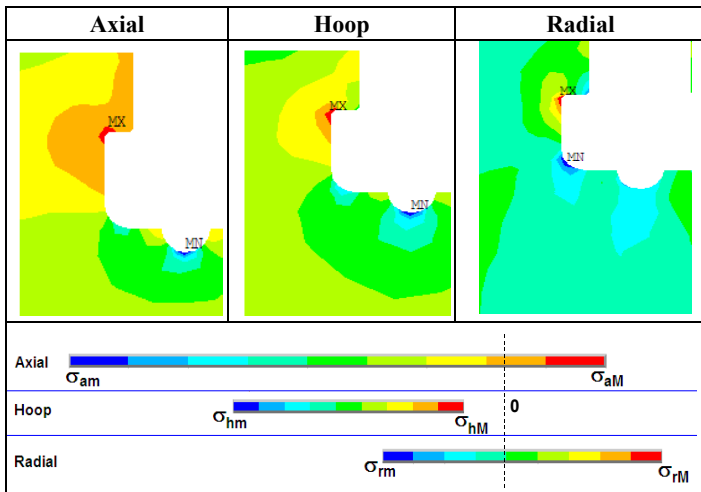


Fig.8 Comparison of stress components at 1st stage groove.

The variation over time of the peak stress at this critical location is depicted in Fig.9, along with the characteristic times t_{w0} , t_{p0} and t_{L0} . It is apparent how, at this location, the initial thermal shock within the first warm-up phase is much more critical than the successive load steps at 15% and up to 100% load.

Despite such high transient elastic stresses disappear, at steady state, in case they overcome yield level, the successive steady state may induce a residual tensile stress that may become critical during the following shutdown phase. Indeed, during cool-down the overall thermal behavior is reversed and elastic tensile stresses are produced at the outer layers. Since the heat transfer coefficients in the cool-down phase are much lower than those during startup, the cool-down stresses are usually not of concern if not superimposed on the residual stresses.

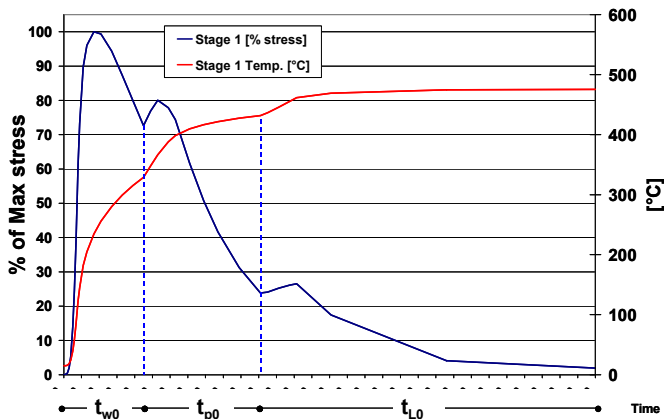


Fig.9 Equivalent Von Mises stress and temperature variation, during startup, at bottom of dovetail groove.

To take all that into account, an elasto-plastic transient analysis was performed showing that a tensile axial residual stress was present at the groove bottom, as represented in Fig. 10.

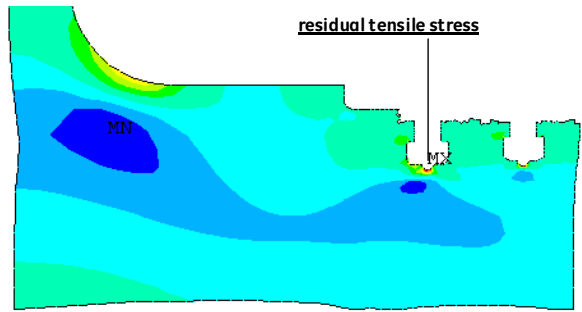


Fig.10 Residual axial tensile stress at steady state

The component life calculation followed the total equivalent strain range approach and Miner’s rule for linear damage accumulation. The details for the application of these classic approaches to component life assessment will not be further detailed in the discussion to follow.

However, the elasto-plastic total equivalent strain range methodology showed that the baseline geometry and proposed startup conditions were not to be recommended for highly cyclic operation due to the risk of an LCF crack initiation and propagation, in the critical locations identified above. Therefore, several improvements were proposed.

5 IMPROVEMENT AREAS

5.1 Locking pin geometry

As discussed above, the grooves for the insertion of blade radial locking crush pins are high stress concentrators during thermal transients. In order to reduce these stresses while keeping the same functionality, an analysis of moving these grooves from the shaft to the lower face of the bucket dovetail was conducted. This reduced by approximately 40% the shaft peak stress at these locations.

After this modification the critical locations in the dovetail grooves became the lower fillets, where both axial and radial stresses persist (ref. Fig.8). As a final local improvement, these areas were further relieved by increasing the fillet radii as much as possible without affecting the bucket geometry.

5.2 Thermal relief groove

Once the above local solutions were implemented, analyses showed that the peak stresses were still located at the bucket dovetail grooves that themselves constitute notch factors. This was especially evident at the 1st stage and, in general, at the extreme stages of each drum, where the axial spacing between the grooves is slightly increased. This spacing is critical because, during thermal transients, the groove walls are compressed or stretched by the adjacent shaft material proportionally to the axial length of the adjacent portions of the shaft.

Since the only stress level of some concern was at the 1st stage, it was decided to reduce the outer layer of the upstream shaft length by creating a groove, whose purpose is to relieve the 1st stage dovetail stresses, by restoring the usual spacing between the shaft grooves.

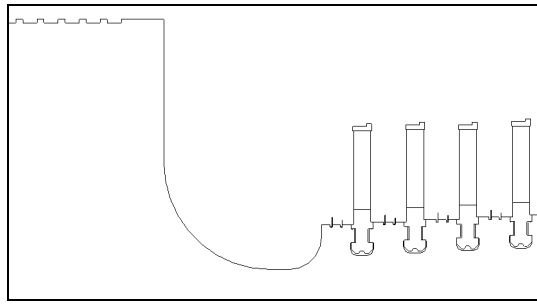


Fig.11 Final improved geometry

The shape of this thermal relief groove was then optimized to :

- minimize stress levels at the groove itself, by adopting the proper fillet radii;
- have a sufficient relief effect at the 1st stage groove by properly selecting the groove depth.

Depending on the size, the thermal relief groove may also be used for ultrasound inspection below the first stage dovetails. Fig.11 shows the overall final geometry that was selected, including all the modifications presented so far.

5.3 Mission / startup cycle

As discussed, the peak stresses are reached at the very beginning of the startup phase and are due to a quite superficial thermal gradient. Since in this initial phase the mass flow is imposed to drive the shaft at warm-up speed, heat transfer coefficients are given as well, and the thermal gradient is mainly driven by the steam temperature.

Another way to reduce the transient thermal shock was to initiate the unit startup with lower steam conditions, as available from the starting of the recovery boiler and properly tuning the gas turbine operation in the combined cycle.

The defined conditions were tested for feasibility for the specific plant in collaboration with the customer, and the resulting data were used as input for the cold startup simulation.

In addition, the times for the warm-up, partial load and final load ramps, as defined in par.3.2, were modified to minimize stresses, as follows.

$t_w = 2 * t_{w0}$	$t_p = t_{p0}$	$t_L = 0,65 * t_{L0}$
--------------------	----------------	-----------------------

These modifications left the overall cold startup time unchanged and reflect the criticality of the initial phase with respect to the final load ramp. The initial warm-up time was increased and the final load ramp is realized faster, while the time for acceleration up to synchronization and partial load operation remained unchanged.

The low pressure section was verified for these modified starting conditions, with respect to possible erosion and windage effects. For erosion, the low peripheral speed and reduced steam pressure compensate for the reduction in inlet temperature, so that the overall final humidity and impact speed at the low pressure blades are reduced with respect to normal operating conditions.

With regard to ventilation effects, the validity of the calculations for prolonged off-design operation, such as during warm-up at low speed, were validated by historical field temperature readings at the exhaust duct. These showed that even with normal starting steam conditions (higher enthalpy), the exhaust temperature reached a steady value well below alarm conditions with no trend to increase.

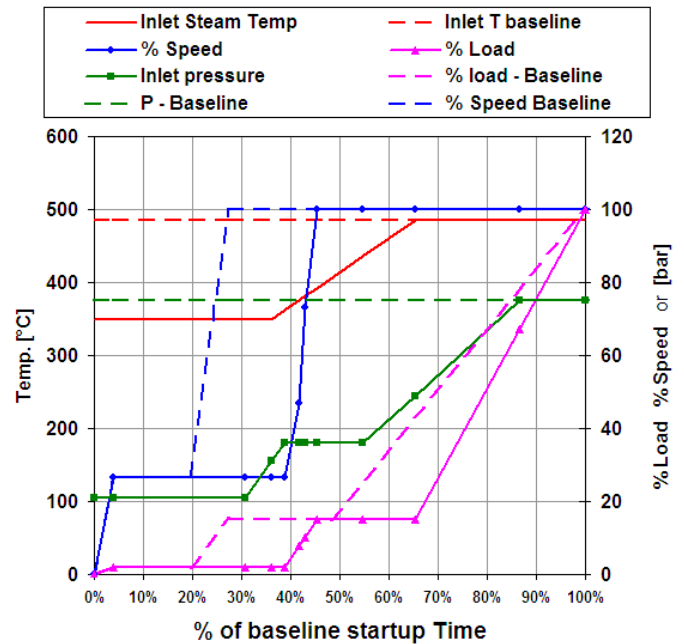


Fig.12 Comparison of Baseline and Modified startup cycles.

Since the modified startup cycle foresees lower temperature and pressure and, consequently, a higher mass flow to keep the same warm-up speed, the new conditions are not expected to be more critical than the normal starting conditions from a windage standpoint.

6 IMPROVED SOLUTION RESULTS

6.1 Thermal distributions

Apart from slower overall thermal gradients due to the softer starting cycle, the only difference worth noting is the local distribution of temperature in the shaft post upstream of the 1st stage. Refer to Fig.13.

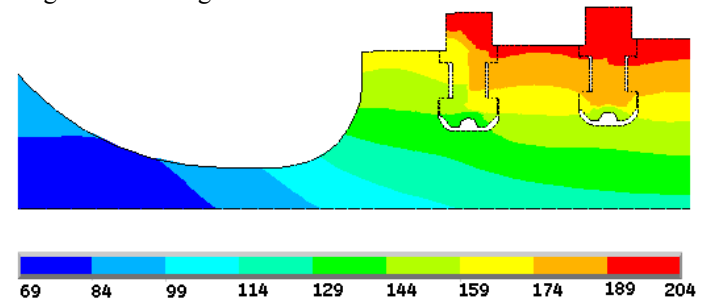


Fig.13 Detail of thermal transient distribution for modified geometry and startup cycle

By comparison with Fig.5 it can be noted that, at the time of maximum stress, the new geometry reaches a more balanced

thermal distribution in the shaft material upstream of the 1st stage, minimizing the surface thermal gradient that is reduced from approximately 70°C of the baseline case (Fig.5) to approximately 30°C for the improved solution.

6.2 Mechanical results

The results of the transient thermomechanical analysis, incorporating all the modifications discussed above, is presented in Fig.14, where the stress distribution in the first stages is reported for the modified geometry and new startup conditions.

The Von Mises equivalent stresses for the new solution (σ_{em} and σ_{eM}) are compared with the baseline results (σ_{em0} and σ_{eM0}), showing that an overall reduction of up to 1/3 of the original peak stress is achieved at this location.

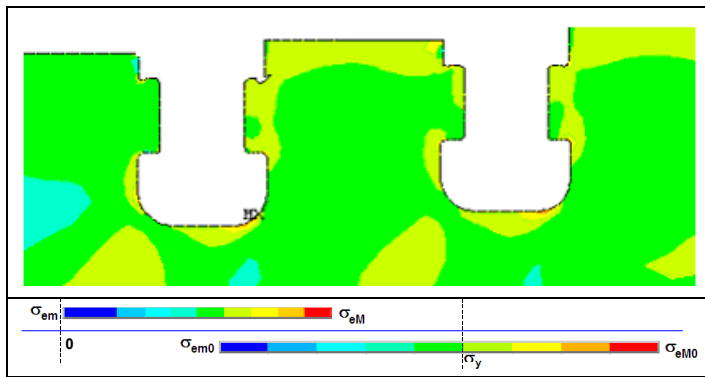


Fig.14 FEM result for the improved solution

For cold starts the peak stresses are still reached at the early phase of startup, even though slightly delayed with respect to the previous case. In addition, the critical shaft location with respect to transient stress is no longer the dovetail groove but has become the thermal relief groove itself and the fillet at the opposite side of the balance drum. In Fig.15, the time variation of these stresses is reported as a percentage of the maximum baseline stress.

A summary of the stress benefits separately provided by each of the improvements discussed is reported in Table 1 as a percentage of the peak von Mises stress reduction.

Improvement	% reduction of von Mises stress
Crush pin groove removal (at 1 st stage)	39%
Thermal relief groove (at 1 st stage)	35%
Soft start (at 1 st stage)	17%
Soft start (at thermal relief groove bottom)	15%
Soft start (at outer balance drum fillet)	37%

Tab.1 Summary of benefits by improvement

The specific results reported above are generalized in the following sections to obtain simplified rules of broad validity for application to sensitivity analyses of the existing fleet or on a job-by-job basis using a simplified approach.

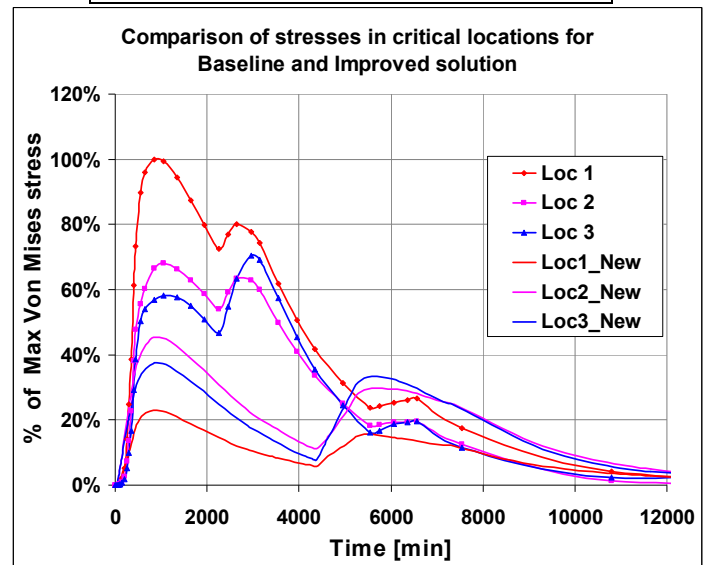
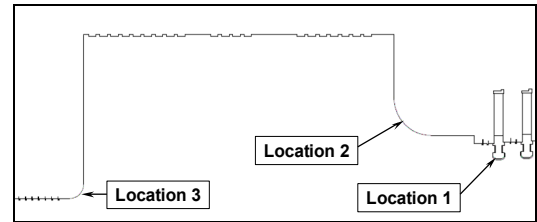


Fig.15 Stress comparison between baseline and improved solution.

7 ANALYTICAL APPROACH

7.1 Approximate thermo-mechanical model

In order to generalize the results of the detailed FEM analysis as well as to conduct a sensitivity analysis of overall stress levels using geometric and thermal parameters, an analytical model was adopted.

Following the approach summarized in [3] and [4], a solid cylinder was used as a simplified rotor model, superimposing transient thermal distributions and mechanical loads where:

- the thermal distribution was obtained by integration of the Fourier equation for heat transfer, cast in cylindrical coordinates, for an infinite full-bore cylinder with no internal heat source [3];
- thermal and centrifugal stresses, depending on speed and transient thermal distribution, were calculated from well established literature formulations [6] at each time step, along the radius.

7.2 Comparison with case study

The results were compared, for several reference points and showed a good fit of the thermal distribution for both the FEM and analytical model. In Fig.16, the comparison of radial temperature distribution at 850[s] from the start is shown for a section of the balance drum.

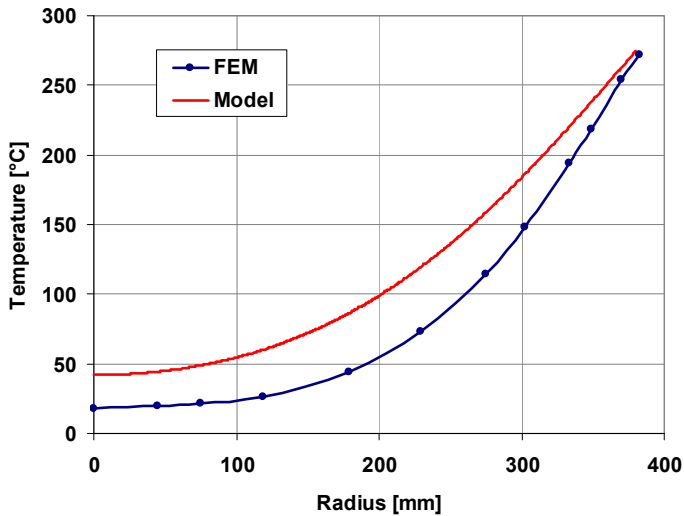


Fig.16 Comparison of transient temperature distribution at 850[s] between FEM result and analytical model.

Similarly, in Fig.17 the stress distributions are compared for the cylindrical region between the balance drum and the 1st stage, these show an acceptable approximation of the FEM results by the approximated model.

The differences are reasonably explained by the model assumptions: the average temperature in Fig.16 is slightly higher for simplified model since the axial heat flow is neglected (heat is not dissipated axially from high temperature locations to the surrounding, colder, sections). Also, the FEM stress distributions show less continuous variations over the radius, capturing the local effects of changes in shaft diameter, across surrounding sections, creating different constraints for axial expansion as well as uneven centrifugal stresses, with respect to the infinite-rod analytical approximation that imposes a plane strain condition.

Despite the closeness of the fit, it is apparent that these stresses are not representative of the actual peak stresses reached at the critical locations identified, such as the grooves or balance drum fillets.

In previous works ([3], [4], [5]), the rotor life computation, as well as the definition of possible real-time supervision systems for the same, were discussed on the basis of a simplified rotor model. However the stresses derived from such models cannot be representative of the actual peak stresses at the critical locations, since their detailed geometry cannot be taken into account.

In this section an attempt to identify the parameters relating the simplified model solutions to the detailed elastic FEM results is carried out. This approach is based on the assumption that the stresses at critical locations (“targets”) can be expressed as functions of “predictors”: stresses at selected locations of the simplified model.

In our case we consider the location corresponding to the bottom of the dovetail groove in the approximate model as predictor for the target stresses of identical location in the shaft and assume that a linear relationship exists between the stress components such as:

$$\sigma_{\text{targ}_i} = K_{\text{th}_i} \sigma_{\text{pred}_i_{\text{th}}} + K_{\text{m}_i} \sigma_{\text{pred}_i_{\text{mech}}} \quad (\text{Eq.1})$$

Where K_{th_i} and K_{m_i} are equivalence factors for stress components i of thermal and mechanical loading origin respectively. These factors depend on the specific geometry of the shaft in the area of interest and on a reference thermal gradient. The evaluation of the K factors is performed first by calculation of K_{m_i} at steady state conditions, when the thermal gradient effect is negligible. Then K_{th_i} is evaluated during the thermal transient, removing the stress contributions due to mechanical loads.

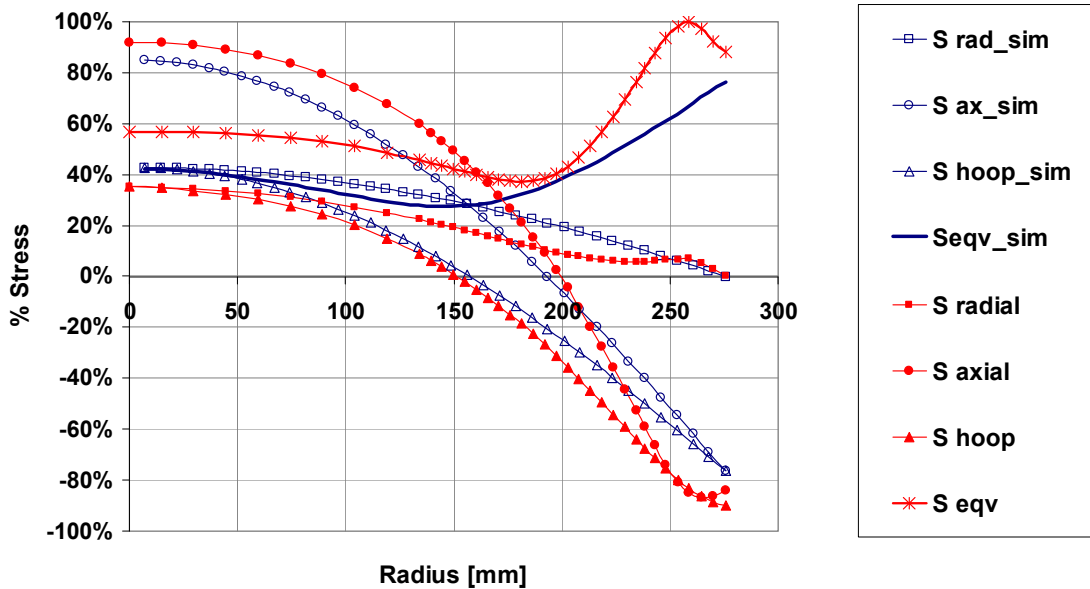


Fig.17 Comparison of transient stresses at 850[s] between FEM result and simplified analytical model, in cylindrical region between balance drum and 1st stage.

In our case the reference thermal gradient is taken as the ratio between the temperature difference from the outer surface to the groove bottom and the groove depth ($\Delta T/\Delta r$). The best fit for K_{th_i} vs. the reference gradient was found to be a linear interpolation :

$$K_{th_i} = a_i (\Delta T/\Delta r) + b_i \quad (\text{Eq.2})$$

Applying these equations to the baseline case we come to the results shown in Fig.18, where the FEM (target) stresses are compared with the values predicted according to Eq.1.

It is worth noting that this approximated approach may be considered viable only when the locations of the predictors are reasonably close to the target ones, or when the temperature variation over time is either very well matched or slow enough to avoid local fluctuations to be interpreted as a high gradient with respect to the target locations.

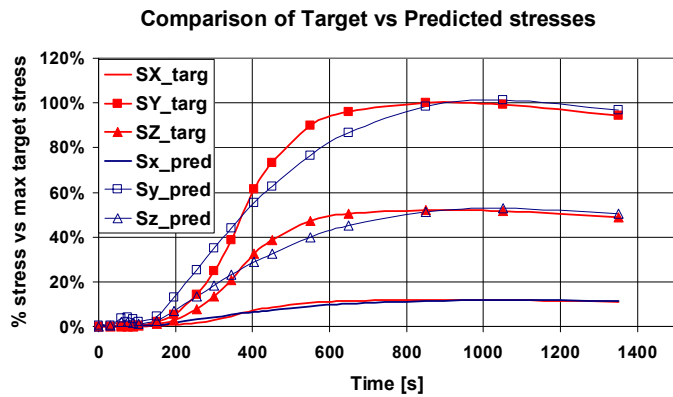


Fig.18 Target vs predicted stresses : x (radial), y(axial), z (hoop).

7.3 Validation

The predictor method described above was tested for different thermal conditions, where results from detailed FEM analyses were already available.

The simulation by the approximate model of the new start-up cycle predicted a reduction of equivalent stress of 19% that closely approximates the reduction of 17% (ref. Tab.1) obtained after a detailed transient thermo-mechanical FEM analysis of the rotor as discussed in par. 6.2.

The ability to quickly evaluate with reasonable accuracy the effects of different thermal and mechanical loading conditions is especially valuable in such cases where it is necessary to account for the sensitivity of the mechanical parameters to operating conditions variability. This happens in many situations, from support to field installations where conditions different from design are found, to sensitivity analyses for conceptual designs or for the evaluation of non conformities.

Once a design is completed, the detailed FEM analyses, developed for the specific geometry and operating conditions, can be used to define equivalence factors for stress predictors at the locations of interest. These are used to tune the

simplified model for matching actual stresses at target locations.

Equivalence factors become “fingerprints”, for the specific design, that depend on the geometry (i.e. different groove shapes) but can be considered invariant with scale and thermal/mechanical load conditions, whose variation is accounted for by the simplified model.

To give a practical perspective of the computational economy of such an approach, consider that each run of the transient thermo mechanical FEM analysis took several hours to complete on a dedicated workstation, while only several seconds are needed for the simplified model to run on a commercial laptop.

Despite this, the described method cannot be considered a detailed design tool, even though it can eliminate the need to run numerous sensitivity analyses recursively, based on computationally heavy and sometimes misused FEM models.

8 APPLICATIONS

8.1 Startup time optimization

As discussed, the need for high cycling operation of machinery comes along with the complimentary requirement of reducing startup times as much as possible to get the maximum economic benefit from on-line time and to provide fast response to peak power needs. This requirement is clear to machinery designers, and some work has been conducted with the aim of linking the overall plant operation (i.e., combined cycles for peak power plants) to the machinery transient stress predictions [5].

In the context of the present work, once the new startup cycle was identified by determining the operating conditions and characteristic times for cold start-up (ref. 5.3), the optimization was aimed at reducing on-line time by tuning starting times based on hot and intermediate conditions.

For hot restart, since there are no idle times for pre-load and warm-up, (they are reduced to the minimum prescribed times necessary for rotor acceleration), the only applicable variable was load time t_l (ref. 3.2). This was defined to limit the peak stresses to the values of cold startup, by dedicated FEM analysis and normal operating steam conditions.

Instead, with reference to restart at intermediate conditions, an estimate of the effects of modifications of characteristic starting times was performed by means of the simplified model introduced above. In particular, the warm-up time t_w was minimized, by determining the lower bound defined by the stresses exceeding the maximum transient values obtained for cold and hot restarts.

As an example, Fig.19 illustrates the result of the optimization of t_w for several different re-start conditions (after 10 to 28 hours of cool down), with respect to the maximum equivalent stress reached at cold start.

From the stress patterns it is apparent how, in the case of hot re-starts, the stresses due to the initial thermal shock may be less than those of successive phases, driven by the increase of load.

In particular, for lower starting temperatures, the warm-up time t_w is progressively increased to begin the successive pre-load phase always at similar shaft thermal conditions, hence keeping the main stress peak within limits. However, by doing so, the 1st stress peak increases as well up to a limit, here shown for curve at 28[h], where both the warm-up and pre-load stress peaks are identical and equal to the upper stress bound. With colder starting conditions it is not possible to further reduce the transient stresses. Indeed, with this starting philosophy, the peak stress during pre-load cannot be reduced below certain thresholds because the steam flow and t_p have a lower bound, driven by the need to accelerate the rotor fast enough to cross the resonance speeds.

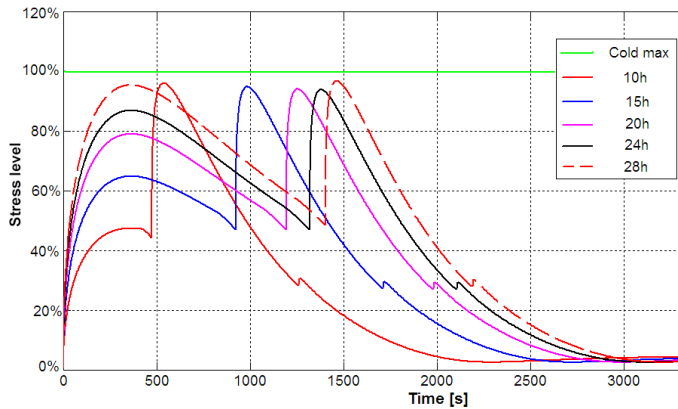


Fig.19 Equivalent transient stress vs max cold start stress for re-starts after different cool down times

With respect to the three-steps starting philosophy discussed above, other approaches foster further starting time reduction by continuously tuning the steam flow to keep the peak stresses almost constantly at the upper allowable bound over the full transient phase. This type of approach implies a very accurate control of the steam conditions and flow and can be very challenging for some applications. This is especially valid for CSPs where steam temperature control is particularly difficult.

9 CONCLUSIONS

The issue of highly cyclic operation of steam turbine rotors was addressed through a case study, with special emphasis on the benefits achievable from improvements to both the shaft geometry and starting parameters. An analytical approach was then introduced for the definition of a simplified model for use in sensitivity analyses to consider thermal and mechanical load variations. This approach was validated by comparison to detailed FEM results and was applied to the preliminary optimization of starting parameters for warm restart conditions.

REFERENCES

- [1] Greenpeace International, Solar PACES and ESTELA, *Global Concentrating Solar Power Outlook 09*. <http://www.greenpeace.org/international/en/publications/reports/concentrating-solar-power-2009/>
- [2] Energy Information Administration, *World Crude Oil Prices*, 2/3/2010 http://tonto.eia.doe.gov/dnav/pet/pet_pri_wco_k_w.htm
- [3] Carnero, P.A., Serrano, R.L., Nebradt, G.J., Leyva M. Luis, Integration of Thermal Stress and Lifetime Supervision System of Steam Turbine Rotors , ASME GT2008, June 9-13, 2008, Berlin, Germany, GT2008-51453.
- [4] Mitrovic, D., Zivkovic, D., Computation of Working Life Consumption of a Steam Turbine Rotor, *Journal of Pressure Vessel Technology*, APRIL 2010, Vol. 132.
- [5] Casella, F., Pretolani, F., Fast Start-up of a Combined-Cycle Power Plant: a Simulation Study with Modelica, Proc. International Modelica Conference, September 4-5, 2006, pp 3-10.
- [6] Young, W.C., Budynas, R.G., *Roark's Formulas for Stress and Strain*, 7th Ed., McGraw-Hill, 2002.